An α-catenin actin-binding domain unfolding mutant designed to lower force-dependent actin-binding promotes epithelial strength but interferes with cell-cell coordination

Megan Wood[1]*, Yuou Wang[1]*, Annette S. Flozak[1], Alex Yemelyanov[1] and Cara J. Gottardi[1,2]**

[1]Department of Pulmonary Medicine, [2]Cell & Developmental Biology,
Northwestern University
Feinberg School of Medicine, Chicago, IL 60611

*Co-first authorship
**Corresponding Author: Cara J. Gottardi
Northwestern University Feinberg School of Medicine
303 Superior St., Simpson-Querrey Institute, 5-525
Chicago, IL 60611
Office Phone: (312) 503-4123

Email: c-gottardi@northwestern.edu
Cara J. Gottardi ORCID: 0000-0003-0912-7617
Yuou Wang ORCID: 0000-0001-8675-8055

Condensed title: α-cat catch-bond in wound repair

Character/Word count: 30,400/5,000 (Excluding References)

ABSTRACT (<200 Words)

α-catenin (α-cat) displays force-dependent binding to actin filaments, but the features of adherens junction structure and function most vulnerable to loss of this allosteric mechanism remain to be generalized across epithelial cell-types. By reconstituting an α-cat F-actin-binding domain unfolding mutant known to exhibit enhanced binding to actin (α-cat-H0-FABD$^+$) into α-cat knock-out Madin Darby Canine Kidney (MDCK) cells, we show that partial loss of the α-cat catch bond mechanism (via an altered H0 α-helix) leads to stronger epithelial sheet integrity with greater co-localization between the α-cat-H0-FABD$^+$ mutant and actin. α-cat-H0-FABD$^+$ -expressing cells are less efficient at closing scratch-wounds or uniformly packing, suggesting reduced capacity for more dynamic cell-cell coordination. Evidence α-cat-H0-FABD$^+$ is equally accessible to the conformationally sensitive α18 antibody epitope as WT α-cat suggests this mutant favors binding to lower tension cortical actin networks. These data suggest signals that reduce the force-sensitivity of the α-cat-cortical actin interaction might improve epithelial monolayer strength through enhanced coupling to lower tension cortical actin networks, but that such association would render α-cat less selective of higher-tension actin networks, extracting a cost for dynamic processes.

INTRODUCTION

α-catenin (α-cat) is a central mechanosensitive scaffold molecule that links the cadherin-catenin complex to the cortical actin cytoskeleton at adherens junctions (AJs), where the latter form structural units essential for tissue morphogenesis and homeostasis (Green et al., 2010; Harris & Tepass, 2010). α-cat mechanosensitivity depends on the conformations and binding activity of its three bundled alpha helical domains (Ishiyama et al., 2013; Rangarajan & Izard, 2012). The N-terminal domain comprises two 4-helical bundles, where the former binds β-catenin (Pokutta & Weis, 2000). The C-terminal domain engages actin through a 5-helical bundle, where force-dependent alteration of the first helix favors high affinity F-actin binding and catch-bond behavior (Buckley et al., 2014; Ishiyama et al., 2018; Wang et al., 2022; Xu et al., 2020). The middle (M)-region of α-cat comprises three 4-helical bundles (M1-3), which undergo sequential unfurling events, M1 at ~5pN forces followed by M2-M3 at ~12pN forces, to recruit α-cat M-domain binding partners in a force-dependent manner (Barrick et al., 2018; Kim et al., 2015; Li et al., 2015; Maki et al., 2018; Pang et al., 2019; Seddiki et al., 2018; Terekhova et al., 2019; Thomas et al., 2013; Yao et al., 2014; Yonemura et al., 2010). As such, α-cat is now understood to be a mechanosensitive protein that links acto-myosin force thresholds to distinct α-cat conformational states and partner recruitment. However, the particular adhesive processes and coordinated behaviors that critically depend on α-cat mechanosensitivity are only just emerging (Cho et al., 2022; Donker et al., 2022; Ishiyama et al., 2018; Matsuzawa et al., 2018; Monster et al., 2021; Noordstra et al., BioRxiv; Sakakibara et al., 2020; Sarpal et al., 2019; Sheppard et al., 2023; Twiss et al., 2012; van den Goor & Miller, 2022).

Our team previously sought to understand the α-cat catch-bond mechanism through a structure-rationalized mutation approach (Ishiyama et al., 2018). By altering 4 amino acids (RAIM to GSGS, a.a. 666-669) in a kinked portion of the first alpha-helix of the α-cat actin-binding domain, Ishiyama et al generated an α-cat with ~3-fold enhanced F-actin binding *in vitro,* suggesting a model for how acto-myosin forces could alter this region and promote strong actin-binding in cells (Ishiyama et al., 2018). Two recent studies extend and refine this model, implicating the entire first α-helix as a force-gate for F-actin binding, where full loss of this domain (a.a. 666-698) leads to substantially higher actin-binding in vitro (18-fold) (Xu et al., 2020), converting a two-state catch bond into a one-state slip bond (Wang et al., 2022). To accommodate these new findings, we now refer to the Ishiyama et al RAIM → GSGS unfolding

mutant as α-cat-H0-FABD$^+$, where H0 refers to a short α-helix preceding the first long helix of the α-cat actin-binding domain. This revised nomenclature allows the field to avoid confusion with the α-cat-ΔH1 mutant of Wang et al (2022), which removes both H0 and H1. Since the α-cat-H0-FABD$^+$ mutant fails to rescue embryonic lethality of zygotic *αCat* null mutant flies, we know this partial catch-bond mechanism is critical for tissue morphogenesis (Ishiyama et al., 2018). But the specific features of AJ structure and epithelial properties most sensitive to partial loss α-cat-ABD F-actin catch-bond behavior are less clear, but important in understanding benefits of such regulation for tissue homeostasis. While our previous work showed that expression of α-cat-H0-FABD$^+$ in α-cat-negative R2/7-variant DLD1 human colon carcinoma cells leads to epithelial monolayers more resistant to shear-forces, but less efficient at wound repair (Ishiyama et al., 2018), the generality and robustness of these findings remain untested.

In the current study, we generalize these findings to another epithelial cell line, Madin Darby Canine Kidney (MDCK). We demonstrate that partial loss of the α-cat catch bond mechanism (via an H0 α-helix unfolding mutant, RAIM → GSGS) leads to stronger epithelial sheet integrity with greater co-localization between α-cat-H0-FABD$^+$ and F-actin, consistent with this mutant's enhanced association with F-actin under solution-binding centrifugation conditions. However, α-cat-H0-FABD$^+$ -expressing cells are less efficient at closing scratch-wounds or uniformly packing, suggested reduced capacity for more dynamic cell-cell coordination. These results suggest that the α-cat catch bond is most critical for dynamic rather than static cell-cell adhesions. Our results further imply that cell signals that might serve to reduce the force-sensitivity of the α-cat/cortical actin interaction would extract a cost for processes relying on dynamic adhesive changes.

121 **RESULTS**

122

123 **An α-cat CRISPR knock-out MDCK cell system to interrogate a α-cat mutant function**

124 To more broadly understand how α-cat force-dependent actin binding contributes to epithelial
125 junction organization and function, we sought to generalize previous efforts with a "force-
126 desensitized" α-cat actin-binding mutant (Ishiyama et al., 2018) to the non-cancerous kidney
127 epithelial cell line, MDCK (Madin Darby Canine Kidney), a widely used cell line in the cell-cell
128 adhesion field. We established α-cat knock-out (KO) MDCK cells using the CRISPR-Cas9
129 system for reconstitution with wild-type or mutant forms of α-cat. We generated RNA guides to
130 α-cat sequences in exons 2 and 4 (Fig. S1A). After transfection and drug selection, single
131 colonies were expanded and screened for lack of α-cat expression. No full length α-cat was
132 detected in knock-out clones by immunoblot analysis (Fig. S1B). Since an immuno-reactive
133 lower molecular weight species was more prominent in clones generated by the most N-terminal
134 guide (gRNA.5), we stably expressed WT α-cat or α-cat-H0-FABD^{+} in the α-cat KO2.2 clone,
135 which expressed this form least. We now know this lower molecular weight species corresponds
136 to a form of α-cat lacking its N-terminal region, likely consequent to our CRISPR-insertion-
137 deletion (INDEL) strategy, which commonly leads to internal ribosome entry and alternative
138 protein products (Tuladhar et al., 2019). As this α-cat isoform lacks the β-cat binding domain
139 and fails to associate with the cadherin-catenin complex, we moved forward with this cell
140 system nonetheless, reasoning this α-cat form cannot directly participate in the cadherin-catenin
141 catch-bond mechanism. Other possible functions of this α-cat isoform and generation of
142 complete α-cat null MDCK clones will be described elsewhere (Flozak et al., in preparation).

143

144 **An α-cat actin-binding domain unfolding mutant with enhanced actin binding increases**
145 **epithelial sheet integrity**

146 Flow sorting the brightest third of α-cat-RFP or -GFP expressing cells (not shown), we
147 generated pooled "polyclonal" cell lines to avoid sub-clone variation. Both RFP and GFP-tagged
148 α-cat proteins were expressed similar to normal α-cat levels seen in parental MDCK cells (Fig.
149 1A). Modestly lower expression of RFP-tagged α-cat proteins may be due to expression from
150 different plasmid promoters (Methods). Consistent with evidence that this α-cat-H0-FABD^{+}

151 (RAIM→GSGS) unfolding mutant favors F-actin binding *in vitro* (Ishiyama et al., 2018), we
152 found that MDCK α-cat-KO2.2 cell monolayers reconstitutied with α-cat-H0-FABD$^+$-GFP
153 remained intact upon dispase treatment and mechanical disruption, whereas WT αCat-GFP
154 restored monolayers dispersed into numerous fragments (Fig. 1B-C). These data are consistent
155 with previous work showing that α-cat-H0-FABD$^+$ enhances monolayer resistance to mechanical
156 disruption in a human colon cancer cell line (Ishiyama et al., 2018), and suggest that reduced
157 force-sensitivity of the α-cat/cortical actin interaction can improve the strength of epithelial
158 sheets across epithelial types.

159

160 **α-cat-H0-FABD$^+$ shows enhanced colocalization with F-actin**

161 Restoration of α-cat-KO MDCK cells with a "force-insensitive" mutant that interrupts α-cat
162 Middle-domain salt-bridge interactions (M319G/R326E) led to enhanced recruitment of F-actin
163 and myosin to cell-cell junctions, presumably via a-cat M-domain binding partners that reinforce
164 and amplify acto-myosin contractility (Matsuzawa et al., 2018). Whether a force-desensitized α-
165 cat-H0-FABD$^+$ with enhanced actin-binding drives similar actin enrichment at junctions is not
166 known. To address this, α-cat KO2.2 cells restored with WT α-cat-RFP or α-cat-H0-FABD$^+$-RFP
167 were grown on Transwell filters for 10 days before fixing and staining with phalloidin. Curiously,
168 these high density cultures revealed non-overlapping patches of WT α-cat and F-actin signal,
169 whereas the α-cat-H0-FABD$^+$ mutant showed smoother alignment (Fig. 2A). Line-scan analysis
170 of representative bicellular junctions (yellow lines) revealed clear spatial segregation of WTα-cat
171 from F-actin, whereas the α-cat-H0-FABD$^+$ mutant distributed more uniformly along F-actin (Fig.
172 2B). Despite the improved colocalization between α-cat-H0-FABD$^+$ and F-actin, total actin levels
173 appeared unaltered in WTα-cat-RFP/α-cat-H0-FABD$^+$-GFP co-cultures (Fig. 2C, x-z views,
174 phalloidin in grayscale). Orthogonal views also showed that while WTα-cat-RFP could apically
175 enrich at the zonula adherens junction, α-cat-H0-FABD$^+$-GFP was distributed more evenly
176 along the lateral membrane, coinciding with F-actin localizations (Fig. 2C, x-z views). Together,
177 these data suggest that the α-cat-H0-FABD$^+$ mutant likely enhances monolayer cohesion by
178 better engaging actin filaments under lower-forces that run along the entire length of the cell-cell
179 contact. Conversely, the WT α-cat is tuned to ignore this pool of actin, engaging only with
180 filaments under higher tension thresholds (e.g., at zonula adherens).

181

182 **α-cat M2-domain is not persistently accessible in α-cat-H0-FABD$^+$**

183 Single molecule stretch measurements along with steered molecular dynamic simulations reveal
184 how the α-cat M-domain may sequentially unfurl under distinct force thresholds (Leckband & de
185 Rooij, 2014; Sheppard et al., 2023). In cells, this M-domain unfurled state has been
186 conveniently detected by the monoclonal antibody, α18, which recognizes an M2-helix (a.a.
187 420-430) preferentially accessible at tension-bearing versus more relaxed cell-cell adhesions
188 (Nagafuchi et al., 1994; Yonemura et al., 2010). Indeed a previous study revealed the M-domain
189 "activated" salt-bridge mutant (M319G/R326E) was substantially more accessible to α18 than
190 WTα-cat (Matsuzawa et al., 2018). To address the extent to which α-cat-H0-FABD$^+$ favors
191 greater accessibility to α18, we co-cultured α-cat-H0-FABD$^+$-GFP with WT α-cat-RFP and
192 stained for α18. We find that while α18 can recognize α-cat-H0-FABD$^+$ better than WT α-cat in
193 some regions of the monolayer (Fig. 3A), other regions showed preferential recognition of WT
194 α-cat by α18 (Fig. 3B). These data reveal that the α-cat M2-domain is not constitutively
195 accessible in α-cat-H0-FABD$^+$, despite its better colocalization with actin, suggesting α18
196 accessibility differences between α-cat-H0-FABD+ and WT α-cat are more likely driven by the
197 complex and variable tension forces experienced by the monolayer. Collectively, these data
198 suggest the α-cat-H0-FABD$^+$ mutant likely engages lower-tension cortical actin networks in
199 dense MDCK monolayers, where these actin networks are typically ignored by WT α-cat.

200

201 **α-cat-H0-FABD$^+$ interferes with normal cell-cell packing**

202 MDCK cells are often used in epithelial biology for their consistent high-density packing on
203 Transwell filters, as evidenced by the normal distribution of apical membrane sizes (Fig. 4A,
204 left). Curiously, MDCK reconstituted with α-cat-H0-FABD$^+$ manifest greater heterogeneity in
205 apical membrane size, with small and large sizes often sharing cell-cell contact (Fig.4A, right).
206 Histogram and Kolmogrov-Smirnov analysis reveal α-cat-H0-FABD$^+$ alters the distribution of
207 apical areas (Fig. 4B & 4C), despite no significant mean apical areas difference between WT α-
208 and α-cat-H0-FABD$^+$ (Fig. 4C). Since this phenomenon can occur in the context of actomyosin
209 contractility differences between adjacent cells (Armon et al., 2018; Matsuzawa et al., 2018),
210 these data suggest an α-cat that is able to engage both lower- and higher-tension actin
211 filaments may be sufficient to propagate signaling relationships that support this irregular cell-
212 packing state.

213 **α-cat-H0-FABD$^+$ limits epithelial sheet wound closure**

214 We previously reported that the α-cat-H0-FABD$^+$ mutant interferes with wound-front migration
215 using the R2/7 DLD1 cell system (Ishiyama et al., 2018), but whether this also holds for MDCK
216 cells, reflecting a generalized phenomenon is unknown. Live imaging of scratch wounded
217 monolayers reveals that α-cat-H0-FABD$^+$ mutant cells display unproductive cell-cell tugging
218 orthogonal to the direction of migration (Fig. 5A), leading to reduced wound area closure than
219 WT α-cat (Fig. 5B & 5C, Movie 1). Finger-like tubular membrane structures, which form via
220 invagination at the interface of leader and follower cells to coordinate directional migration
221 (Hayer et al., 2016), were prominently detected in both WT α-cat and α-cat-H0-FABD$^+$
222 monolayers (Fig. 5A). While some α-cat-H0-FABD$^+$ tubular structures appeared less dynamic
223 and more persistent than WT α-cat (Fig. S2A), there was no significant difference in their
224 number or length (Fig. S2B-C, n = ~50 structures). Interestingly, a greater number of tubular
225 invaginations in α-cat-H0-FABD$^+$ wound fronts were angled perpendicularly to the direction
226 migration, consistent with the more uncoordinated (side-to-side) movements of α-cat-H0-FABD$^+$
227 cells relative to WT α-cat (Fig. S2D-E). These data demonstrate that normal α-cat catch-bond
228 behavior is required for efficient epithelial sheet migration, through favoring a more directional
229 (front-to-back) migration.

230

231

232

233

Discussion

A number of single molecule studies have shown that α-cat binding to F-actin is force-dependent (Arbore et al., 2022; Buckley et al., 2014; Mei et al., 2020), where the first extended α-helix (H0-H1) of α-cat's 5-helical bundle actin-binding domain negatively regulates (i.e., force-gates) actin-binding (Ishiyama et al., 2018; Wang et al., 2022; Xu et al., 2020). However, the features of epithelial junction organization and dynamic cell behaviors that critically depend on α-cat/FABD$^+$ catch-bond activity remain unclear. While our previous work showed that restoring α-cat-H0-FABD$^+$ in an α-cat-negative colon carcinoma cell line led to epithelial monolayers more resistant to shear-forces, but less efficient at wound repair (Ishiyama et al., 2018), the generality and robustness of these phenotypes remained untested. Here, we extend these findings to the MDCK epithelial cell line. We show that partial loss of the α-cat catch bond property (via an altered H0 α-helix) leads to stronger epithelial sheet integrity with greater co-localization between α-cat-H0-FABD$^+$ and F-actin, presumably due to the latter's persistent association with lower tension cortical actin networks. Since α-cat-H0-FABD$^+$ -expressing cells are less efficient at closing scratch-wounds or uniformly packing at high density, this mutant displays reduced capacity for dynamic cell-cell coordination. These results reinforce the idea that the α-cat catch bond mechanism is most critical for dynamic rather than static cell-cell adhesions. These results further imply an interesting trade-off-- Cell signals (heretofore unknown) that serve to reduce the force-sensitivity of the α-cat/cortical actin interaction might improve epithelial monolayer strength through enhanced binding to lower tension cortical actin networks. Indeed these lower tension actin networks may comprise the bulk of cortical actin in mature epithelial monolayers. But such signals would render α-cat less selective of acto-myosin filaments under higher force, extracting a cost for more dynamic processes, such as collective cell migrations, which depend on α-cat ignoring the lower tension actin networks,.

A limitation of relying on the α-cat-H0-FABD$^+$ mutant to infer α-cat catch-bond activity in cells is the current lack of information on its force-dependent activity using optical trap single molecule analyses (Fig. S3). WT α-cat manifests two-state binding to actin: low or no binding under low forces, binding under mid-forces and slippage under high forces (Arbore et al., 2022; Buckley et al., 2014). Recent studies suggest this two-state model property implicates both H0 and H1, but largely centers on the longer H1 helix (Mei et al., 2020; Wang et al., 2022; Xu et al., 2020).

265 Deletion of both helices (ΔH0-H1 ABD) leads to greatly enhanced actin binding in solution (18-
266 fold; Xu et al., 2020) and longer binding lifetimes under low forces, but "slippage" at mid-range
267 forces (Wang et al., 2022). As the α-cat-H0-FABD$^+$ mutant shows more modest increase in F-
268 actin binding affinity *in vitro* (3-4-fold, (Ishiyama et al., 2018) versus 18x (Xu et al., 2020)), it is
269 likely this mutant still manifests two-state catch bond activity, as the vinculin ABD also lacks H0,
270 yet nonetheless forms catch-bonds with actin (Bakolitsa et al., 1999, 2004; Borgon et al., 2004;
271 Huang et al., 2017). We reason, therefore, that the α-cat-H0-FABD$^+$ mutant interacts with actin
272 under lower force thresholds in cells. This model is supported by the enhanced colocalization of
273 α-cat-H0-FABD$^+$ with lateral membrane F-actin compared with WT α-cat, where the latter
274 accumulates in membrane patches that exclude actin (Fig. 2). Moreover, evidence the M2-
275 domain α18 epitope is not constitutively accessible at α-cat-H0-FABD$^+$ compared with WT α-cat
276 cell-cell junctions further supports the idea that α-cat-H0-FABD$^+$ largely engages lower tension
277 cortical actin networks (Fig. 6, Schematic). Taken together, we speculate the α-cat-H0-FABD+
278 mutant behaves as a "force-desensitized" form of α-cat in epithelial cells, but the particular
279 force-sensitive profile of this mutant will require future testing.

280

281 We were intrigued that cells expressing the α-cat-H0-FABD$^+$ mutant led to non-normal packing
282 distribution of MDCK cells grown to high density on filters, where cells with small apically
283 constricted junctions were directly connected to seemingly larger flatter cells (Fig. 4A). Indeed,
284 tissues can adopt this packing state under different conditions (Armon et al., 2018) and via
285 altered expression of junction proteins and signaling relationships that impact apical contractility
286 (Hildebrand, 2005; Matsuzawa et al., 2021; Sakakibara et al., 2020). Evidence here suggests
287 the that an α-cat with enhanced binding to lower tension actin networks with possible slippage
288 under higher forces may be sufficient to propagate similar cell-cell relationships.

289

290 A recent study found MCF7 α-cat KO cells reconstituted with α-cat H0-FABD$^+$ showed
291 enhanced adherens junction assembly during the last step of epithelial wound-front closure,
292 where "head-on" junction establishment was associated with reduced lamellipodial activity and
293 cortical actin flow (Noordstra et al., BioRxiv). Interestingly, unliganded surface E-cadherin
294 moved faster in MCF7 cells reconstituted with α-cat H0-FABD$^+$, with no change in the overall
295 speed of cortical actin flow. We speculate this enhancement in α-cat H0-FABD$^+$ cortical flow

296 may be due to increased binding to lower tension actin networks. Conversely, cortical flow was
297 impeded if cells were directly imaged on E-cad-Fc substrate, suggesting homophilic E-cadherin
298 engagement can alter the cadherin-catenin complex in a manner that ultimately reduces actin
299 flows (e.g. via cadherin clustering) (Noordstra et al., BioRxiv). While we find no consistent
300 differences in α-cat cluster size along lateral contacts of mature or wounded MDCK monolayers
301 (Figs. 2&5), higher resolution imaging may be required. As more biophysical data become
302 available on the α-cat H0-FABD^{+} (or other) catch-bond mutants, the field can better understand
303 the interplay of acto-myosin force on α-cat actin-binding properties and adherens junction
304 regulation.

305

306 **Study Limitations:** This study relies on α-cat constructs with GFP or RFP-tags placed at the
307 carboxyl-terminus, based on evidence that αCat null flies are fully rescued by an αCat-GFP
308 transgene (Sarpal et al., 2012). Since the unstructured C-terminal extension also contributes to
309 force-activated actin binding (Mei et al., 2020), and the extreme C-terminus of α-cat contains a
310 PDZ-interaction motif, likely blocked by placement of these tags, some adherens junction
311 functionalities and phenotypes may be missed in this study.

312

313

314 **ACKNOWLEDGEMENTS**

315 This work relied on the following Northwestern University services and core facilities: Flow
316 Cytometry (NCI CA060553); Center for Advanced Microscopy (NCI CCSG P30 CA060553) and
317 Skin Biology and Diseases Resource-based Center (P30AR075049) from the NIAMS. We thank
318 Pankaj Bhalla for gene editing advice with help from the SBDRC GET iN Core.

319

320 **FUNDING**

321 CJG is supported by NIH GM129312. All authors declare no competing financial interests.

322

323 **Author contributions**: MNW, ASF and AY conducted experiments; MNW, ASF and AY, YW
324 and CJG analyzed results; CJG designed and supervised the study. YW and CJG wrote the
325 manuscript. CJG provided funding for project.

326 **METHODS**

327 *Plasmid generation and constructs*

328 The αE-catenin cDNA was amplified by PCR and subcloned into either a modified pcDNA3.1
329 vector (Ishiyama et al., 2010) to express αE-catenin-mRFP or a modified pCAN vector (Ichii &
330 Takeichi, 2007) to express αE-catenin-mEGFP (EGFP with the dimerization-disrupting A206K
331 mutation (Zacharias et al., 2002)).

332

333 *Cell culture and stable cell line selection*

334 MDCK II cells were maintained in Dulbecco's Modified Eagle's Medium (DMEM, Corning),
335 containing 10% fetal bovine serum (FBS, Atlanta Biologicals or JRS Scientific), 100 U/ml
336 penicillin and 100 μg/ml streptomycin (Corning). α-cat/*Ctnna1* knockout MDCK cells were
337 generated using CRISPR-Cas9 system, RNA guides were designed targeting α-cat sequences
338 in exons 2 and 4. Guide RNA (gRNA) targeting different canine *CTNNA1* exons were designed
339 with CHOPCHOP online tools.[45] Sequences of oligonucleotides were as follows: 5'-
340 GAAAATGACTTCTGTCCACACAGG -3' (exon 2, covering the MTSVHTG protein sequence)
341 and 5'-AGTCTAGAGATCCGAACTCTGG -3' (exon 2, covering the SLEIRTLA sequence).
342 Single guide RNA (sgRNA), Cas9 nuclease (HiFi) and duplex buffer were purchased from
343 Integrated DNA Technologies. RNAs were reconstituted and diluted to 5 μM with duplex buffer;
344 Cas9 protein to 10 μM with PBS. MDCK cells were plated in 12-well plates at a seeding density
345 of 1.0 x 10^5 cells in 1 mL DMEM-complete a day before. For one reaction, sgRNA (20 μL), Cas9
346 (15 μL), DMEM (30 μL, no serum and antibiotics) and Lipofectamine RNAiMax (4 μL, Invitrogen)
347 were mixed and incubated at room temperature for 20 min. The complex was treated to the cells
348 in complete medium and incubated overnight at 37 °C and 5% CO_2. The medium was changed
349 and the cells were allowed to recover for one day. Cells were split to maintain 30-50%
350 confluency. The sgRNA-Cas9 treatment was repeated 3 times. Cells were expanded and sorted
351 with a flow cytometer (FACSMelody, BD) to 96-well plates to grow single cell colonies. The
352 colonies were screened for low (< 5 ng/well at confluent) α-cat expression using a α-cat C-
353 terminal antibodies. The selected colonies were verified with western blot. Knockout cell line
354 (2.2 clone) was chosen based on lowest level of α-cat isoform lacking N-terminal sequences.

355

356 After transfection and drug selection, colonies were expanded and screened for lack of α-cat
357 expression. Cells were transfected with expression vectors by using Lipofectamine 3000
358 (ThermoFisher Scientific), and cells with stable protein expression was selected based on
359 antibiotic resistance (100 µg/mL Zeocin for pcDNA3.1 and 300 µg/mL hygromycin for pCAH
360 vectors) and subsequently isolated by flow cytometry.

361

362 *Antibodies*

363 The following primary antibodies were used: polyclonal rabbit anti-α-cat (C3236, Cell Signaling),
364 hybridoma mouse anti-α-catenin (5B11,(Daugherty et al., 2014)), Rat anti-α-catenin mAb (α18)
365 was a kind gift of Dr. A. Nagafuchi (Nara Medical University, Nara, Japan), rabbit anti-GAPDH
366 (Cat# sc-25778, Santa Cruz, now discontinued), polyclonal rabbit anti-GFP (A11122, Invitrogen)
367 and Phalloidin-488 or -568 (A12379, Invitrogen). Secondary antibodies for Western blotting
368 included HRP-conjugated goat anti-mouse and -rabbit antibodies (Bio-Rad), or fluorescently
369 labeled donkey anti-mouse and -rabbit antibodies (680RD or 800RD, LiCor Biosciences).
370 Secondary antibodies for immunofluorescence included IgG Alexa Fluor 488 or 568-conjugated
371 goat anti-mouse or -rabbit antibodies (Invitrogen).

372

373 *Immunofluorescence and Imaging*

374 Cells were grown on cell culture inserts (Falcon), fixed in 4% paraformaldehyde (Electron
375 Microscopy Services, Hatfield, PA) for 15', quenched with glycine, permeabilized with 0.3%
376 Triton X-100 (Sigma), and blocked with normal goat serum (Sigma). Primary and secondary
377 antibody incubations were performed at RT for 1h, interspaced by multiple washes in PBS, and
378 followed by mounting coverslips in ProLong Gold fixative (Life Technologies). Images of α-cat &
379 F-actin localizations were captured with Nikon A1R Confocal Laser Point Scanning microscope
380 using NIS Elements software (Nikon) with GaAsP detectors and equipped with 95B prime
381 Photometrics camera, Plan-Apochromat 60x/1.4 objective. Confocal Z-stacks were taken at step
382 size of 0.3µm.

383

384 *Scratch Wound Assay*

385 MDCK cells (250,000) were plated for 24hr on LabTek #1 4-well chamber slide (43300-776,
386 ThermoScientific), wounded with a P200 micropipette tip and allowed to recover for 2hr. Prior to
387 imaging, DMEM media was replaced with FluoroBright DMEM (Life Technologies) and 10
388 μg/mL Mitomycin C (Sigma) to limit cell proliferation. Cells in Figure 5 were imaged with the 20x
389 objective every 10 min (both phase contrast and fluorescent channels) on the Nikon Biostation
390 IM-Q with the slide holder module (located in Nikon Imaging Facility) at 37°C, 5% CO_2, for 15 hr.
391 6 fields of view (FOV) were captured along the wound edge. To quantify change in wound area,
392 the resulting .ids file was imported to ImageJ, and the wound edge of the phase-contrast image
393 was traced with the polygon tool at time = 0 and time = 15hr. The area of the resulting polygon
394 was measured in pixels² and the resulting data were compared by performing One-way ANOVA
395 statistical analysis followed by Tukey's multiple comparison test using GraphPad. Images
396 presented in the paper were adjusted for brightness/contrast but were otherwise unprocessed.
397 Individual cell tracks were visualized using the MTrackJ plug-in (FIJI) (Supplementary Fig. 5E).
398 Cadherin fingers were counted manually and within 150-minutes after wounding. Length,
399 intensity & angles were measured using FIJI by using the line tool (line width of 3 pixels) along
400 the cadherin fingers at 200% zoom.

401

402 *Epithelial sheet disruption assay*

403 350,000 cells were plated in a 12-well culture plates (Corning) and allowed to reach confluency.
404 36hr post-plating, the monolayer was washed 2x in DPBS supplemented with 0.5 mM Mg^{++} and
405 1 mM Ca^{++} (HyClone) and then incubated for 30 min at 37°C in 1 mg/ml Dispase (Roche)
406 diluted in PBS (Corning) and supplemented with the indicated amount of Ca^{++}. After monolayers
407 lifted from the dish, the plate was subjected to a shaking force of 1400 rpm for 15 sec. An image
408 of each well was captured before and after shaking, and the resulting file names were blinded
409 (RandomNames Script from HowToGeek.com) prior to counting each fragment with the multi-
410 point marker in ImageJ. Seventy-five epithelial fragments were established as the upper limit for
411 counting. The assay was repeated with 3 BR and combined counts for each Ca^{++} condition was
412 compared with an unpaired t-test.

413

414

415

416 **Key resources Table**

REAGENT or RESOURCE	SOURCE	IDENTIFIER
Antibodies		
Anti-α-catenin	Cell Signaling	Cat#3236
Anti-α-catenin (5B11)		https://www.pnas.org/doi/10.1073/pnas.1308663111
Anti-α-catenin (α18)		Dr. A. Nagafuchi (Nara Medical University, Nara, Japan)
GAPDH	Santa Cruz	Cat# sc-25778
Anti-GFP	Invitrogen	A11122
Alexa Fluro 568 phalloidin	Invitrogen	Cat#A12380
Alexa Fluro 488 phalloidin	Invitrogen	Cat#A12379
Goat anti-rabbit Alexa Fluor 488	Invitrogen	Cat#A11008
Goat anti-mouse Alexa Fluor 568	Invitrogen	Cat#A11004
HRP-conjugated goat anti-mouse	BioRad	Cat#1706516
HRP-conjugated goat anti-rabbit	BioRad	Cat#1706515
Donkey anti-mouse	LiCor Biosciences	P/N 925-68072
Donkey anti-rabbit	LiCor Biosciences	P/N: 926-32213
Chemicals, Peptides, and Recombinant Proteins		
Hoechst 33342	ThermoFisher Scientific	Cat#62249
ProLong Gold Antifade Mountant	ThermoFisher Scientific	Cat#P36934
Dispase	Corning	Cat#47743-724
Critical Commercial Assays		
Experimental Models: Organisms/Strains		
Madin-Darby canine kidney II cells	Gumbiner Lab (1996)	Heidelberg strain (Kai Simmons Lab)
Software and Algorithms		
FIJI/ImageJ (version: 2.1.0/1.53c)	Schneider, CA et al., 2012	https://imagej.nih.gov/ij/
Stardist plugin	Schmit, U et al., 2018	Cell/nuclear size quantification https://arxiv.org/abs/1806.03535
Graphpad Prism		https://www.graphpad.com/scientific-software/prism/
Other		
BioStation Slide Holder	Nikon Instruments	
Axioplan2 epifluorescence microscope	Zeiss; 20x objective (Air)	AxioCAM HR Camera with AxioVision 4.8 software
A1R Confocal	Nikon Instruments	Laser Point Scanning, GaAsP detectors, Plan-Apochromat 60x/1.4 objective
Plasmids		
αE-catenin-mRFP in pcDNA3.1	Invitrogen	Ishiyama et al., 2018
αE-catenin-mGFP in modified pCAN	Modified pCAN vector (Ichii & Takeichi, 2007)	Ishiyama et al., 2018; eGFP with the dimerization-disrupting A206K mutation(Zacharias et al., 2002)).

417

418 **FIGURE LEGENDS**

419

420 **Figure S1: Generation of α-cat knock-out MDCK cells via CRISPR-Cas9.** (**A**) Schematic
421 shows location of guide RNAs (gRNA.5 and gRNA.2) targeting MTSVHTGN translational start
422 site protein sequence within exon2 of *CTNNA1* gene. (**B**) Immunoblot characterization of
423 clonally expanded α-catenin knock-out lines 5.1, 5.2, 2.1 and 2.2 from gRNA.5 or gRNA2,
424 respectively. Note that gRNA5 led to clones robustly expressing an α-cat fragment (*) likely
425 generated by an alternative translational start site (Bullions et al., 1997). Therefore, we chose to
426 restore wild-type (WT) α-cat and mutant using α-cat KO clone 2.2. MDCK-parental cell line
427 shown as control (clone 2.2* denotes clone used for reconstitution in this study).

428

A

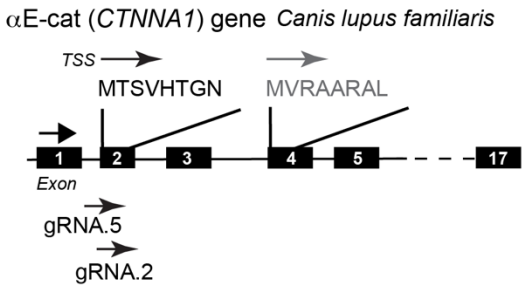

B

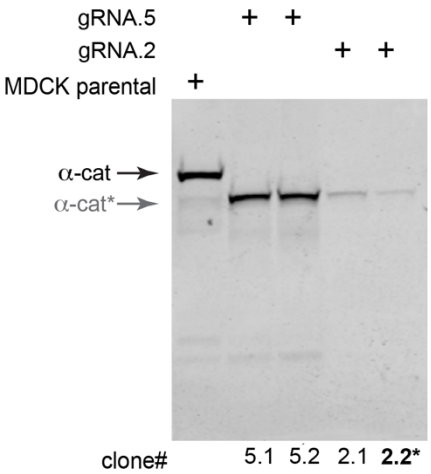

429

Figure 1: An α-cat actin-binding domain unfolding mutant with enhanced binding to lower-tension actin filaments increases cell-cell adhesive strength. (**A**) Immunoblot of MDCK KO2.2 cells transfected with RFP or GFP-tagged versions of WT α-cat or an F-actin-binding-domain (FABD) unfolding mutant (α-cat-H0-FABD$^+$). GAPDH was used as loading control. (**B**) Epithelial sheet disruption assay of MDCK KO2.2 cells expressing WT α-cat (top) or α-cat-H0-FABD$^+$ (bottom). Representative monolayers after mechanical stress treatment under a gradient of calcium concentrations (to sensitize calcium-sensitive, cadherin homophilic binding activity) are shown. (**C**) Quantification of monolayer fragments after mechanical disruption using an orbital shaker. Error bars show mean ± SD (n=3, technical replicates), ****p<0.0001, paired t-test.

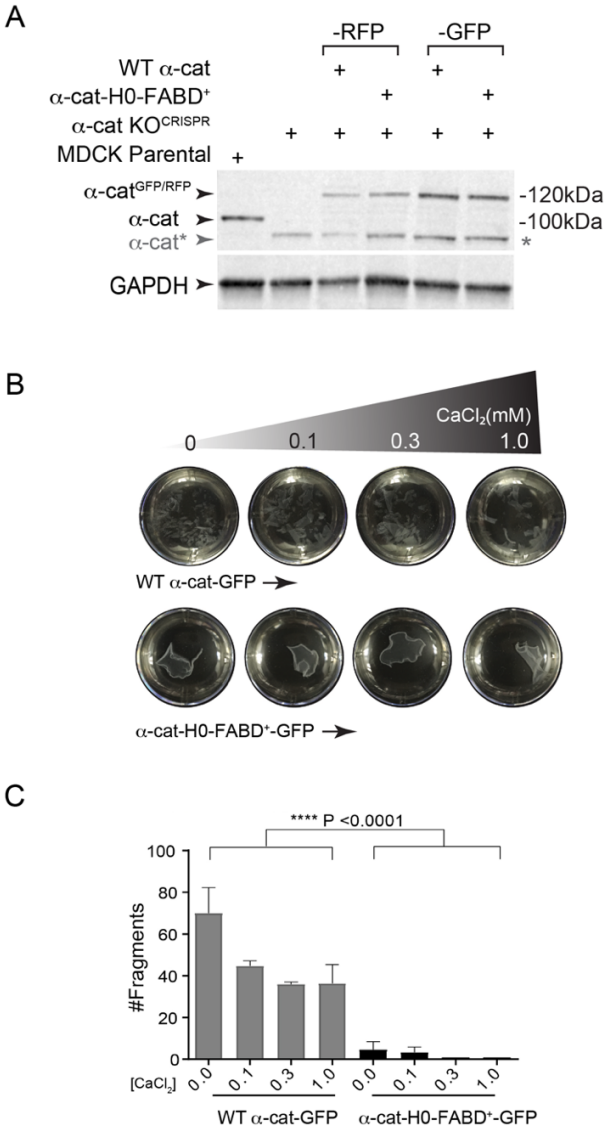

Figure 2: α-cat-H0-FABD$^+$ enhances colocalization with F-actin in MDCK cells.

(**A**) WT α-cat-RFP and α-cat-H0-FABD$^+$-RFP MDCK monolayers (10-12 days on Transwell 0.4μm filters) were stained for phalloidin. Maximum intensity projections of confocal images and representative x-z orthogonal images (white arrowhead denotes section line) are shown. Bars, 10μm. (**B**) Intensity profiles of α-cat-RFP and F-actin along bicellular junctions (yellow lines in A). (**C**) WT α-cat-RFP and α-cat-H0-FABD$^+$-GFP were co-cultured and stained for phalloidin (phalloidin shown in grayscale). Representative x-z orthogonal images are shown. Bar, 10μm.

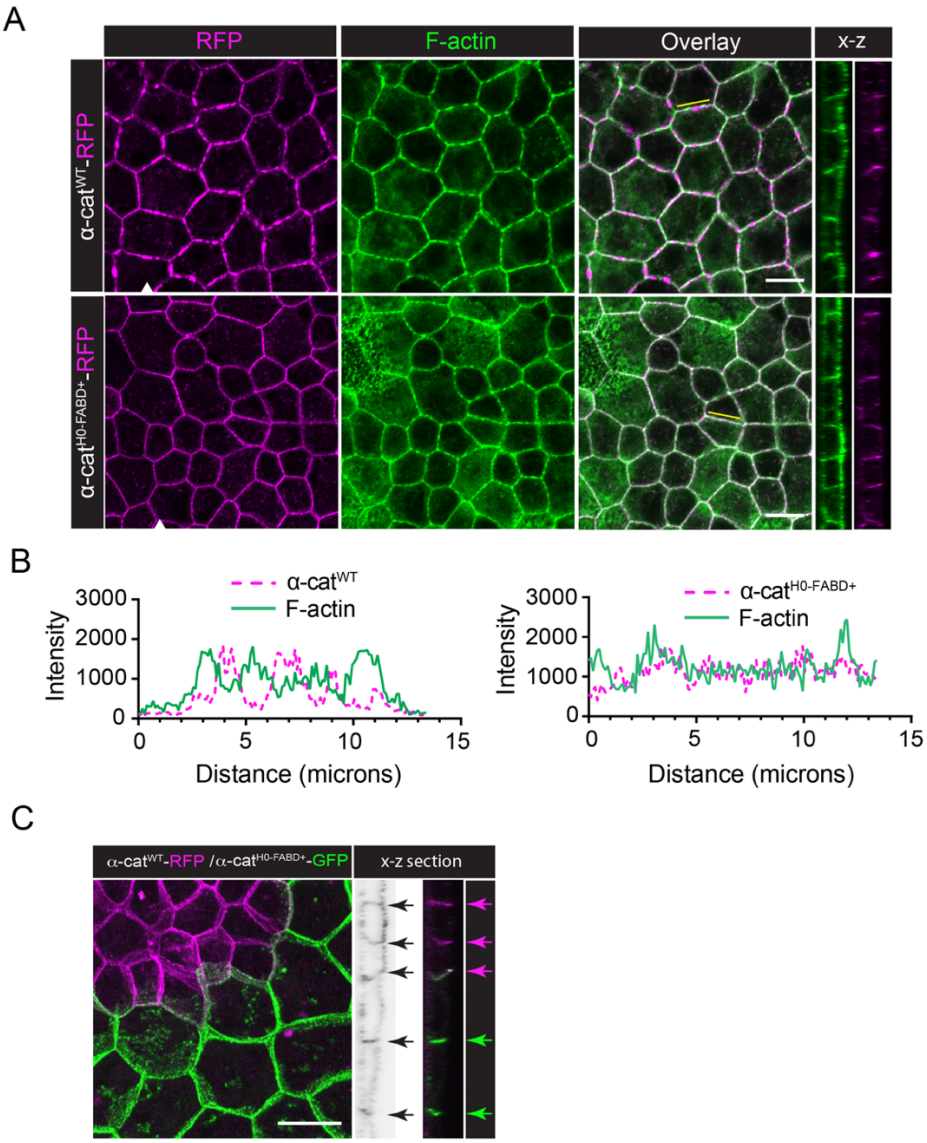

451 **Figure 3: α-cat M2-domain α-18 epitope shows no preference for α-cat-H0-FABD^{+} over**
452 **WT-α-cat.** (**A, B**) WT α-cat-RFP (magenta) and α-cat-H0-FABD^{+}-GFP (green) were co-cultured
453 on Transwell filters for 10-12 days, fixed and stained with α18 monoclonal antibody (grayscale).
454 Representative x-z orthogonal images are shown (horizontal dotted line shows section line).
455 Insets (i) and (ii) show zoomed-in views (right). Bar, 10μm.

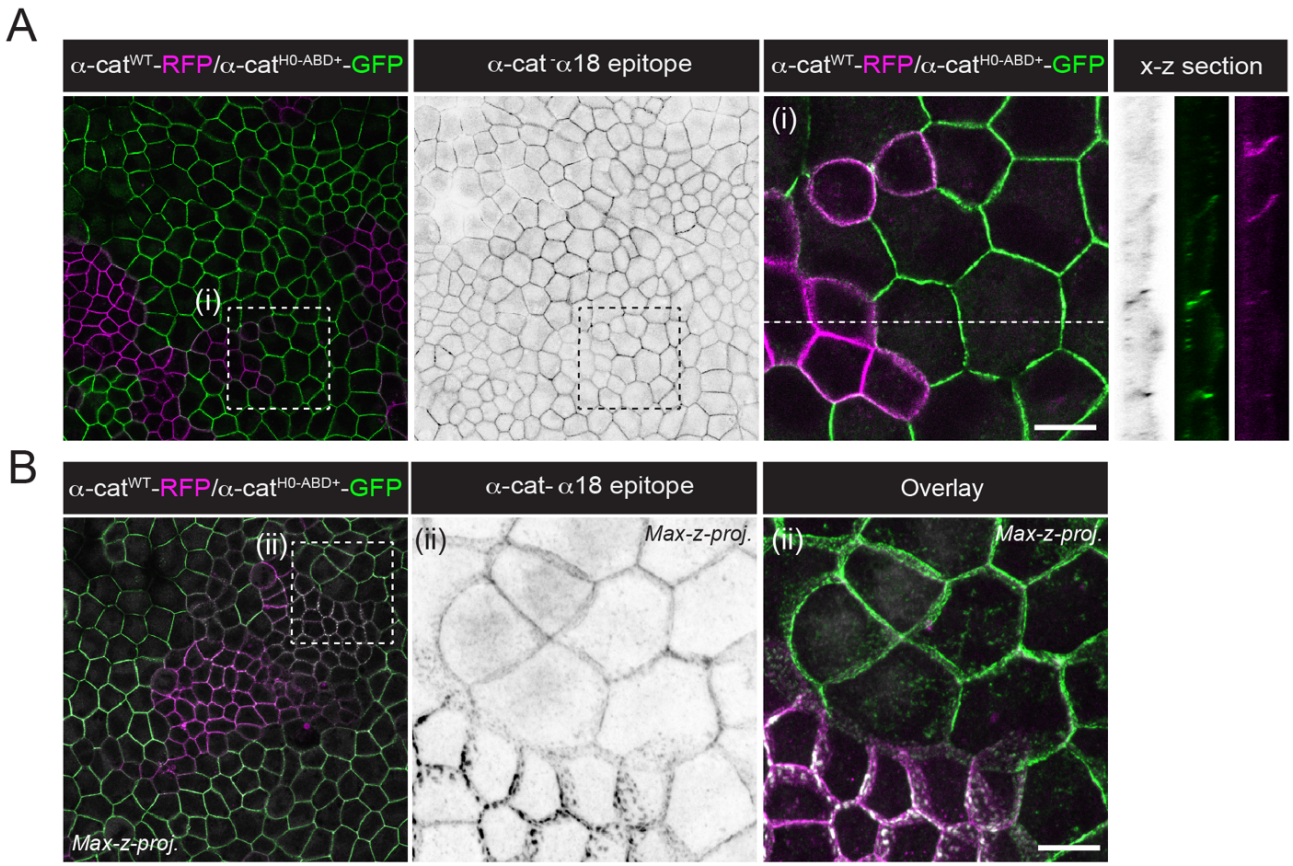

456

457

Figure 4: α-cat-H0-FABD$^+$ interferes with normal packing of MDCK cells.

(**A**) WT α-cat-RFP and α-cat-H0-FABD$^+$-RFP -expressing MDCK monolayers (matured 12-days on Transwell 0.4μm filters, magenta) were fixed and stained with phalloidin (green). Magenta asterisk indicates cells with extra small apical area; white asterisk indicates cells with extra larger area. Bar, 10μm. (**B**) Cell number distributions of apical areas in WT α-cat-RFP and α-cat-H0-FABD$^+$-RFP cells. Data from three independent FOVs using FIJI-StarDist plug-in. (**C**) Violin plot of apical areas in WT α-cat-RFP and α-cat-H0-FABD$^+$-RFP cells. Mean apical areas are not significantly different by unpaired t-test, but the distribution of apical areas (**B**) is significantly different by Kolmogrov-Smirnov analysis (****p < 0.0001).

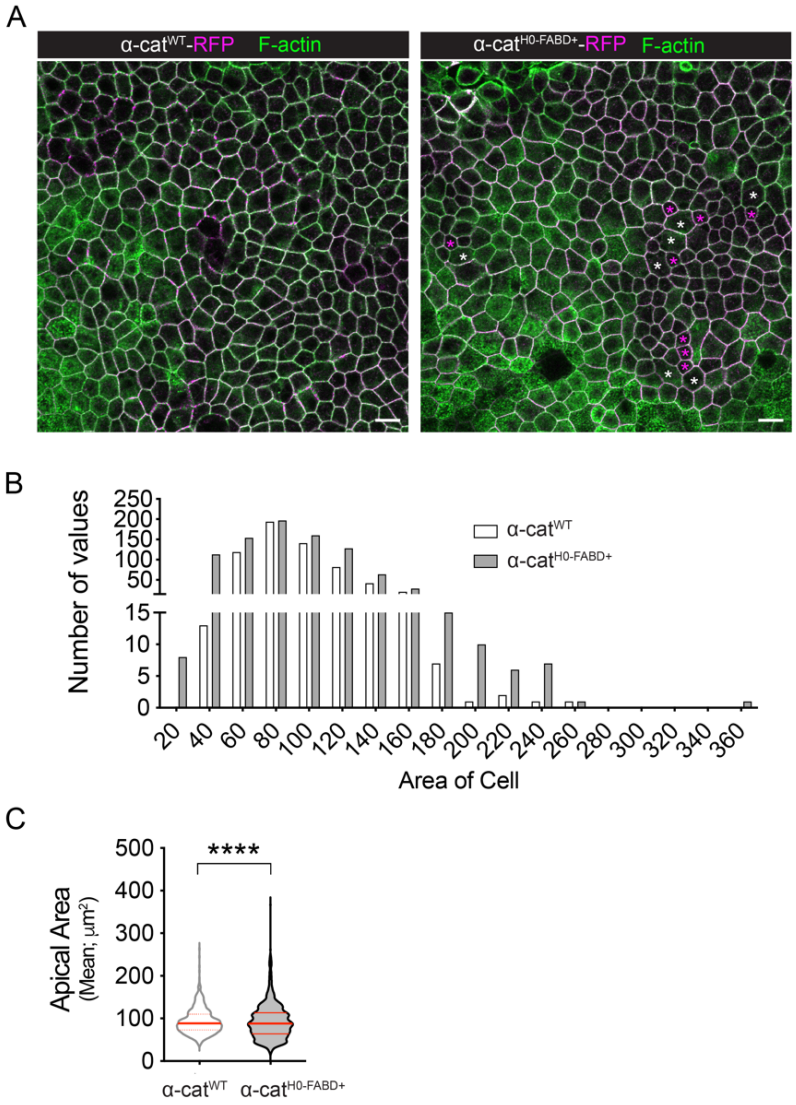

469 **Figure 5: α-cat-H0-FABD⁺ slows MDCK epithelial sheet wound closure.**

470 (**A**) Scratch wound healing assays with MDCK KO2.2 cells restored with WT α-cat-GFP or α-
471 cat-H0-FABD⁺-GFP. GFP signals at wound front area at 0-hr or 8-hr are shown. Zoom-in views
472 (i and ii) show "finger-like" protrusions (green arrows). (**B**) Dot distribution plot showing wound
473 closure area covered by WT α-cat-GFP or α-cat-H0-FABD⁺-GFP after 8hrs. Data from three
474 independent repeats, mean ±SD. ****p<0.0001 by ANOVA. (**C**) Representative plot traces
475 showing faster migration rate of WT α-cat-GFP versus α-cat-H0-FABD⁺-GFP cells throughout
476 an entire time-course.

477

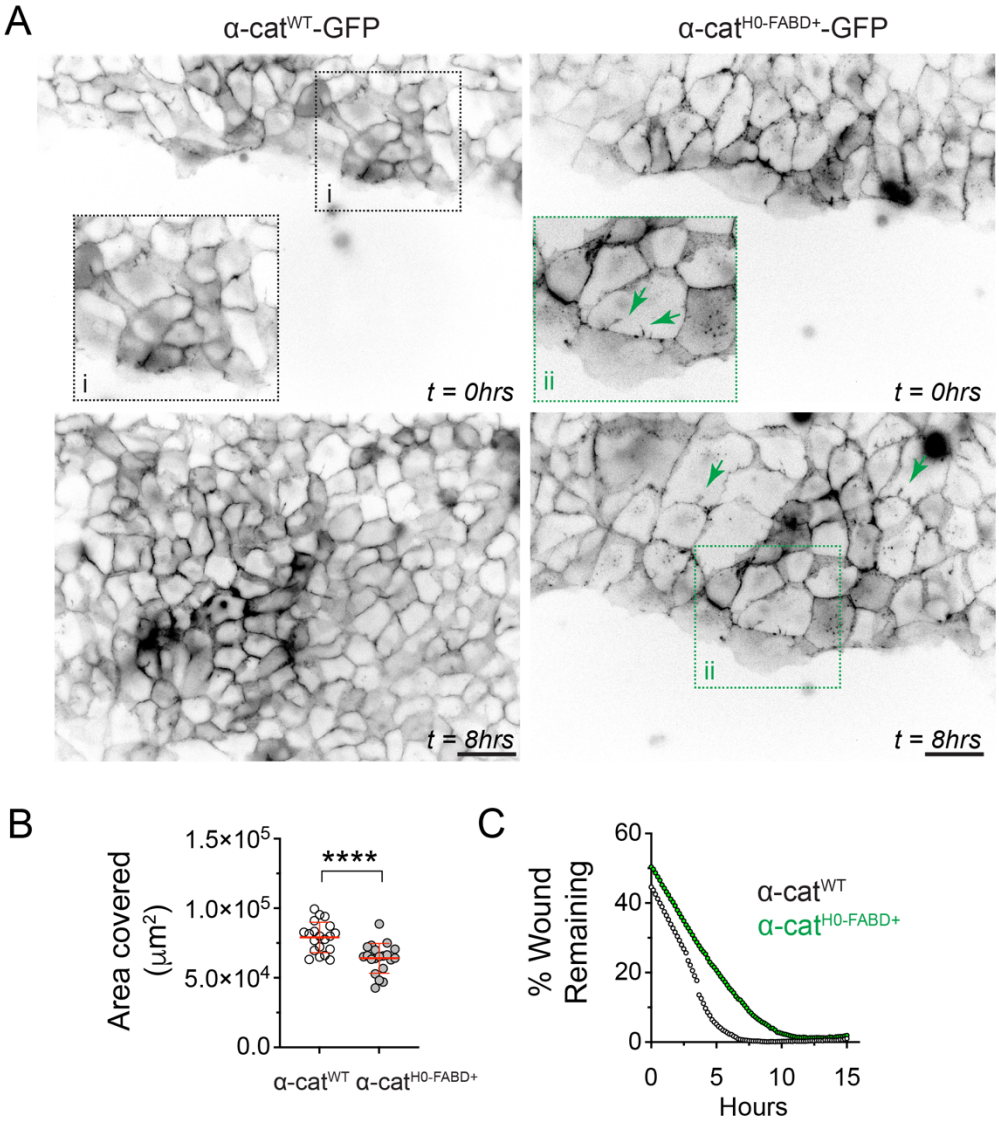

478

Figure S2: Finger-like tubular invaginations form equally between WT α-cat and α-cat-H0-FABD⁺ expressing MDCK wound front leader and follower cells. (A) Time-lapse images of MDCK KO2.2 cells restored with WT α-cat-GFP or α-cat-H0-FABD⁺-GFP. Native GFP fluorescence shown in grayscale (inverted). Cyan arrows points to finger-like invaginations at interface between leader cell and follower cell. Scale bar, 5μm. (**B-D**) Quantification of tubular invaginations (n = 51 for WT α-cat and 46 for α-cat-H0-FABD⁺: (**B**) Length, unpaired t-test, p = 0.4101; (**C**) Fluorescence intensity, unpaired t-test, p = 0.3477; (**D**) Direction/angle formed by tubular invagination and direction of sheet migration, Kolmogorov-Smirnov test, where asterisk (*) reflects p = 0.0408. (**E**) Representative WT-α-cat tubular invaginations align with direction of migration (phase image, colored tracks); α-cat-H0-FABD⁺ invaginations align perpendicular to direction of migration.

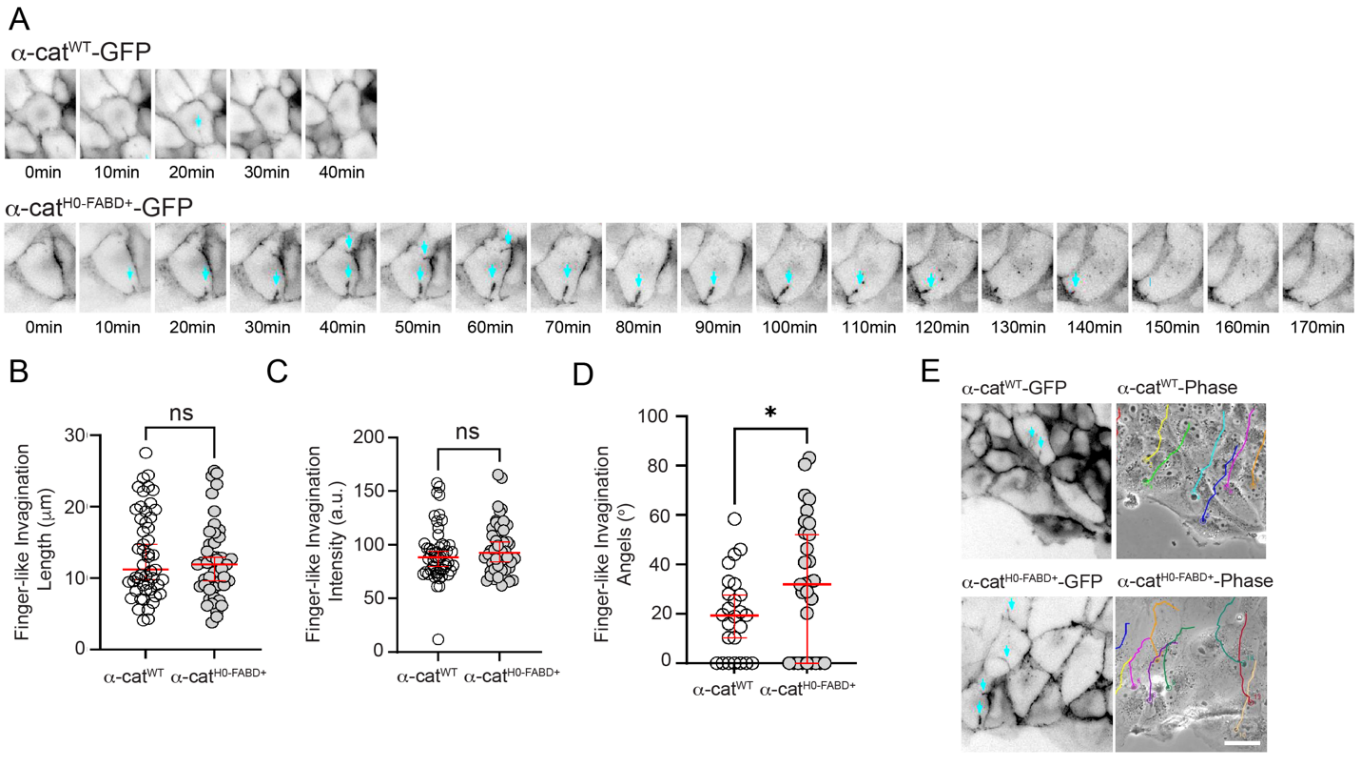

Figure S3: Schematic of α-cat actin-binding domain (ABD) mutants and properties used in this study. (**Left**) Schematic of WT α-cat actin-binding domain based on crystallographic structure, which reveals bundle of 5 helices and an unstructured C-terminal extension (CTE) (Ishiyama et al., 2013, 2018; Rangarajan & Izard, 2012). WT α-cat shows low affinity binding to F-actin in solution (Actin-pelleting Assay, Kd = 8.5μM) and two-state binding by single molecule force-trap measurements (Buckley et al., 2014, Xu et al., 2020, Wang et al., 2022). (**Middle**) Schematic of α-cat-H0-ABD protein designed by Ishiyama et al (2018) to unfold the short H0-helix. This mutant shows enhanced binding to F-actin in solution (Kd = 2μM). Single molecule force-trap measurements remain untested for this mutant; two-state binding is likely possible based similarity to vinculin. (**Right**) The α-cat-ΔH0-H1-ABD protein of Wang et al (2022) removes both H0-H1 helices. This mutant shows dramatically enhanced (18-fold) binding to F-actin in solution (Kd = 0.5μM) and one-state slip-binding by single molecule force-trap measurements (Wang et al., 2022). Cell based studies carried out here (MDCK cells) and elsewhere (colon carcinoma cell line, Ishiyama et al., 2018) suggest the α-cat-H0-ABD mutant is less force-"discriminating" or "selective" of actin filaments than WT α-cat protein, with implications for static versus dynamic cell-cell behaviors.

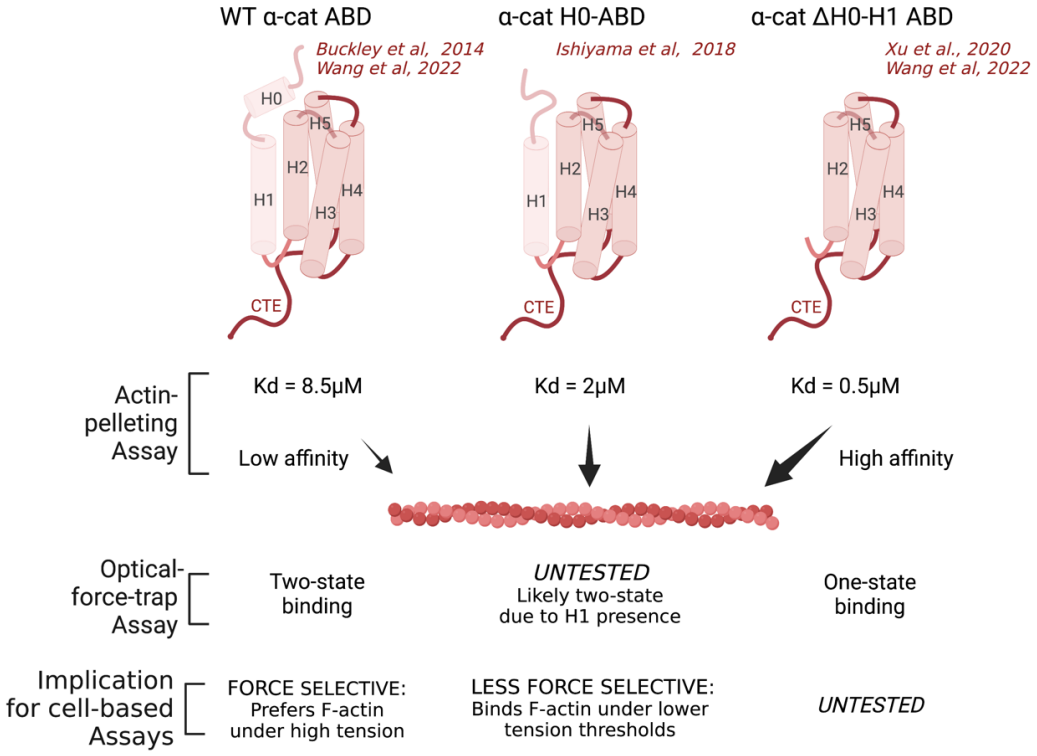

Figure 6: MODEL: Force-desensitized α-cat-H0-FABD$^+$ enhances epithelial sheet strength but interferes with cell-cell coordination during wound-closure.

(**A**) Schematic of WT α-cat FABD (red segment of multicolor α-cat protein) binding an actin filament under low tension (left) or high tension (right). “No/weak binding” vs “strong binding” arrows (red) are based on affinity measurements of Buckley et al., 2014 and Wang et al., 2022 (shown in Fig. S3). (**B**) Schematic of α-cat-H0-FABD$^+$ protein binding actin filament under low or no tension (left) based on affinity measurements of Ishiyama et al., 2018. Tension-dependent affinity change remains untested for α-cat-H0-FABD$^+$ protein, but speculated based on α-cat-ΔH0-H1-FABD$^+$ protein analysis of Wang et al., 2022 (also in Fig. S3). Similar α18 monoclonal antibody accessibility observed for both WT α-cat and α-cat-H0-FABD$^+$ (Fig. 3) is consistent with notion that α-cat-H0-FABD$^+$ engages cortical actin-filaments under lower-tension. (**C**) Consequence of a “force-desensitized” α-cat mutant for epithelial properties: Static epithelial sheet strength is increased, but dynamic sheet migration is antagonized due to reduced acto-myosin force-selectivity, which perturbs cell-cell coordination.

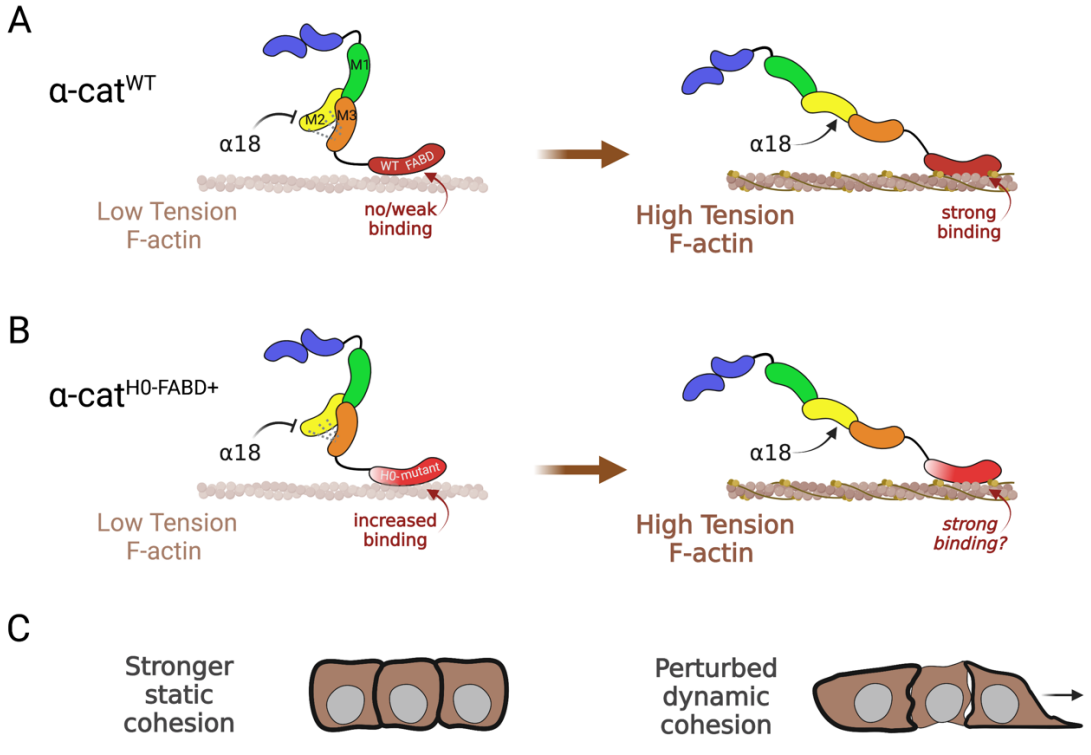

527 **REFERENCES**

528 Arbore, C., Sergides, M., Gardini, L., Bianchi, G., Kashchuk, A. v., Pertici, I., Bianco, P., Pavone, F. S., &
529 Capitanio, M. (2022). α-catenin switches between a slip and an asymmetric catch bond with F-actin
530 to cooperatively regulate cell junction fluidity. *Nature Communications*, *13*(1), 1146.
531 https://doi.org/10.1038/s41467-022-28779-7

532 Armon, S., Bull, M. S., Aranda-Diaz, A., & Prakash, M. (2018). Ultrafast epithelial contractions provide
533 insights into contraction speed limits and tissue integrity. *Proceedings of the National Academy of*
534 *Sciences*, *115*(44). https://doi.org/10.1073/pnas.1802934115

535 Bakolitsa, C., Cohen, D. M., Bankston, L. A., Bobkov, A. A., Cadwell, G. W., Jennings, L., Critchley, D. R.,
536 Craig, S. W., & Liddington, R. C. (2004). Structural basis for vinculin activation at sites of cell
537 adhesion. *Nature*, *430*(6999), 583–586. https://doi.org/10.1038/nature02610

538 Bakolitsa, C., de Pereda, J. M., Bagshaw, C. R., Critchley, D. R., & Liddington, R. C. (1999). Crystal
539 Structure of the Vinculin Tail Suggests a Pathway for Activation. *Cell*, *99*(6), 603–613.
540 https://doi.org/10.1016/S0092-8674(00)81549-4

541 Barrick, S., Li, J., Kong, X., Ray, A., Tajkhorshid, E., & Leckband, D. (2018). Salt bridges gate α-catenin
542 activation at intercellular junctions. *Molecular Biology of the Cell*, *29*(2), 111–122.
543 https://doi.org/10.1091/mbc.E17-03-0168

544 Borgon, R. A., Vonrhein, C., Bricogne, G., Bois, P. R. J., & Izard, T. (2004). Crystal Structure of Human
545 Vinculin. *Structure*, *12*(7), 1189–1197. https://doi.org/10.1016/j.str.2004.05.009

546 Buckley, C. D., Tan, J., Anderson, K. L., Hanein, D., Volkmann, N., Weis, W. I., Nelson, W. J., & Dunn, A.
547 R. (2014). Cell adhesion. The minimal cadherin-catenin complex binds to actin filaments under
548 force. *Science (New York, N.Y.)*, *346*(6209), 1254211. https://doi.org/10.1126/science.1254211

549 Bullions, L. C., Notterman, D. A., Chung, L. S., & Levine, A. J. (1997). Expression of wild-type alpha-
550 catenin protein in cells with a mutant alpha-catenin gene restores both growth regulation and tumor
551 suppressor activities. *Molecular and Cellular Biology*, *17*(8), 4501–4508.
552 https://doi.org/10.1128/MCB.17.8.4501

553 Cho, Y., Haraguchi, D., Shigetomi, K., Matsuzawa, K., Uchida, S., & Ikenouchi, J. (2022). Tricellulin
554 secures the epithelial barrier at tricellular junctions by interacting with actomyosin. *Journal of Cell*
555 *Biology*, *221*(4). https://doi.org/10.1083/jcb.202009037

556 Daugherty, R. L., Serebryannyy, L., Yemelyanov, A., Flozak, A. S., Yu, H.-J., Kosak, S. T., deLanerolle,
557 P., & Gottardi, C. J. (2014). α-Catenin is an inhibitor of transcription. *Proceedings of the National*
558 *Academy of Sciences*, *111*(14), 5260–5265. https://doi.org/10.1073/pnas.1308663111

559 Donker, L., Houtekamer, R., Vliem, M., Sipieter, F., Canever, H., Gómez-González, M., Bosch-Padrós,
560 M., Pannekoek, W.-J., Trepat, X., Borghi, N., & Gloerich, M. (2022). A mechanical G2 checkpoint
561 controls epithelial cell division through E-cadherin-mediated regulation of Wee1-Cdk1. *Cell Reports*,
562 *41*(2), 111475. https://doi.org/10.1016/j.celrep.2022.111475

563 Green, K. J., Getsios, S., Troyanovsky, S., & Godsel, L. M. (2010). Intercellular junction assembly,
564 dynamics, and homeostasis. *Cold Spring Harbor Perspectives in Biology*, *2*(2), a000125.
565 https://doi.org/10.1101/cshperspect.a000125

566 Harris, T. J. C., & Tepass, U. (2010). Adherens junctions: from molecules to morphogenesis. *Nature*
567 *Reviews. Molecular Cell Biology*, *11*(7), 502–514. https://doi.org/10.1038/nrm2927

568 Hayer, A., Shao, L., Chung, M., Joubert, L.-M., Yang, H. W., Tsai, F.-C., Bisaria, A., Betzig, E., & Meyer,
569 T. (2016). Engulfed cadherin fingers are polarized junctional structures between collectively
570 migrating endothelial cells. *Nature Cell Biology*, *18*(12), 1311–1323. https://doi.org/10.1038/ncb3438

571 Hildebrand, J. D. (2005). Shroom regulates epithelial cell shape via the apical positioning of an
572 actomyosin network. *Journal of Cell Science*, *118*(22), 5191–5203. https://doi.org/10.1242/jcs.02626

573 Huang, D. L., Bax, N. A., Buckley, C. D., Weis, W. I., & Dunn, A. R. (2017). Vinculin forms a directionally
574 asymmetric catch bond with F-actin. *Science*, *357*(6352), 703–706.
575 https://doi.org/10.1126/science.aan2556

576 Ichii, T., & Takeichi, M. (2007). p120-catenin regulates microtubule dynamics and cell migration in a
577 cadherin-independent manner. *Genes to Cells*, *12*(7), 827–839. https://doi.org/10.1111/j.1365-
578 2443.2007.01095.x

579 Ishiyama, N., Lee, S.-H., Liu, S., Li, G.-Y., Smith, M. J., Reichardt, L. F., & Ikura, M. (2010). Dynamic and
580 Static Interactions between p120 Catenin and E-Cadherin Regulate the Stability of Cell-Cell
581 Adhesion. *Cell*, *141*(1), 117–128. https://doi.org/10.1016/j.cell.2010.01.017

582 Ishiyama, N., Sarpal, R., Wood, M. N., Barrick, S. K., Nishikawa, T., Hayashi, H., Kobb, A. B., Flozak, A.
583 S., Yemelyanov, A., Fernandez-Gonzalez, R., Yonemura, S., Leckband, D. E., Gottardi, C. J.,
584 Tepass, U., & Ikura, M. (2018). Force-dependent allostery of the α-catenin actin-binding domain
585 controls adherens junction dynamics and functions. *Nature Communications*, *9*(1), 5121.
586 https://doi.org/10.1038/s41467-018-07481-7

587 Ishiyama, N., Tanaka, N., Abe, K., Yang, Y. J., Abbas, Y. M., Umitsu, M., Nagar, B., Bueler, S. A.,
588 Rubinstein, J. L., Takeichi, M., & Ikura, M. (2013). An autoinhibited structure of α-catenin and its
589 implications for vinculin recruitment to adherens junctions. *The Journal of Biological Chemistry*,
590 *288*(22), 15913–15925. https://doi.org/10.1074/jbc.M113.453928

591 Kim, T.-J., Zheng, S., Sun, J., Muhamed, I., Wu, J., Lei, L., Kong, X., Leckband, D. E., & Wang, Y. (2015).
592 Dynamic Visualization of α-Catenin Reveals Rapid, Reversible Conformation Switching between
593 Tension States. *Current Biology*, *25*(2), 218–224. https://doi.org/10.1016/j.cub.2014.11.017

594 Leckband, D. E., & de Rooij, J. (2014). Cadherin Adhesion and Mechanotransduction. *Annual Review of*
595 *Cell and Developmental Biology*, *30*(1), 291–315. https://doi.org/10.1146/annurev-cellbio-100913-
596 013212

597 Li, J., Newhall, J., Ishiyama, N., Gottardi, C., Ikura, M., Leckband, D. E., & Tajkhorshid, E. (2015).
598 Structural Determinants of the Mechanical Stability of α-Catenin. *Journal of Biological Chemistry*,
599 *290*(31), 18890–18903. https://doi.org/10.1074/jbc.M115.647941

600 Maki, K., Han, S.-W., Hirano, Y., Yonemura, S., Hakoshima, T., & Adachi, T. (2018). Real-time TIRF
601 observation of vinculin recruitment to stretched α-catenin by AFM. *Scientific Reports*, *8*(1), 1575.
602 https://doi.org/10.1038/s41598-018-20115-8

603 Matsuzawa, K., Himoto, T., Mochizuki, Y., & Ikenouchi, J. (2018). α-Catenin Controls the Anisotropy of
604 Force Distribution at Cell-Cell Junctions during Collective Cell Migration. *Cell Reports*, *23*(12),
605 3447–3456. https://doi.org/10.1016/j.celrep.2018.05.070

606 Matsuzawa, K., Ohga, H., Shigetomi, K., Shiiya, T., Hirashima, M., & Ikenouchi, J. (2021). MAGIs
607 regulate aPKC to enable balanced distribution of intercellular tension for epithelial sheet
608 homeostasis. *Communications Biology*, *4*(1), 337. https://doi.org/10.1038/s42003-021-01874-z

Mei, L., Espinosa de los Reyes, S., Reynolds, M. J., Leicher, R., Liu, S., & Alushin, G. M. (2020). Molecular mechanism for direct actin force-sensing by α-catenin. *ELife*, *9*. https://doi.org/10.7554/eLife.62514

Monster, J. L., Donker, L., Vliem, M. J., Win, Z., Matthews, H. K., Cheah, J. S., Yamada, S., de Rooij, J., Baum, B., & Gloerich, M. (2021). An asymmetric junctional mechanoresponse coordinates mitotic rounding with epithelial integrity. *Journal of Cell Biology*, *220*(5). https://doi.org/10.1083/jcb.202001042

Nagafuchi, A., Ishihara, S., & Tsukita, S. (1994). The roles of catenins in the cadherin-mediated cell adhesion: functional analysis of E-cadherin-alpha catenin fusion molecules. *Journal of Cell Biology*, *127*(1), 235–245. https://doi.org/10.1083/jcb.127.1.235

Noordstra, I., Díez Hermoso, M., Schimmel, L., Bonfim-Melo, A., Kalappurakkal, J. M., Mayor, S., Gordon, E., Cusachs, P. R., & Yap, A. S. (n.d.). *Cortical actin flow activates an a-catenin clutch to assemble adherens junctions*. https://doi.org/10.1101/2021.07.28.454239

Pang, S. M., Le, S., Kwiatkowski, A. v., & Yan, J. (2019). Mechanical stability of αT-catenin and its activation by force for vinculin binding. *Molecular Biology of the Cell*, *30*(16), 1930–1937. https://doi.org/10.1091/mbc.E19-02-0102

Pokutta, S., & Weis, W. I. (2000). Structure of the dimerization and beta-catenin-binding region of alpha-catenin. *Molecular Cell*, *5*(3), 533–543. https://doi.org/10.1016/s1097-2765(00)80447-5

Rangarajan, E. S., & Izard, T. (2012). The cytoskeletal protein α-catenin unfurls upon binding to vinculin. *The Journal of Biological Chemistry*, *287*(22), 18492–18499. https://doi.org/10.1074/jbc.M112.351023

Sakakibara, S., Mizutani, K., Sugiura, A., Sakane, A., Sasaki, T., Yonemura, S., & Takai, Y. (2020). Afadin regulates actomyosin organization through αE-catenin at adherens junctions. *Journal of Cell Biology*, *219*(5). https://doi.org/10.1083/jcb.201907079

Sarpal, R., Pellikka, M., Patel, R. R., Hui, F. Y. W., Godt, D., & Tepass, U. (2012). Mutational analysis supports a core role for *Drosophila* α-Catenin in adherens junction function. *Journal of Cell Science*, *125*(1), 233–245. https://doi.org/10.1242/jcs.096644

Sarpal, R., Yan, V., Kazakova, L., Sheppard, L., Yu, J. C., Fernandez-Gonzalez, R., & Tepass, U. (2019). Role of α-Catenin and its mechanosensing properties in regulating Hippo/YAP-dependent tissue growth. *PLOS Genetics*, *15*(11), e1008454. https://doi.org/10.1371/journal.pgen.1008454

Seddiki, R., Narayana, G. H. N. S., Strale, P.-O., Balcioglu, H. E., Peyret, G., Yao, M., Le, A. P., Teck Lim, C., Yan, J., Ladoux, B., & Mège, R. M. (2018). Force-dependent binding of vinculin to α-catenin regulates cell–cell contact stability and collective cell behavior. *Molecular Biology of the Cell*, *29*(4), 380–388. https://doi.org/10.1091/mbc.E17-04-0231

Sheppard, L., Green, D. G., Lerchbaumer, G., Rothenberg, K. E., Fernandez-Gonzalez, R., & Tepass, U. (2023). The α-Catenin mechanosensing M region is required for cell adhesion during tissue morphogenesis. *The Journal of Cell Biology*, *222*(2). https://doi.org/10.1083/jcb.202108091

Terekhova, K., Pokutta, S., Kee, Y. S., Li, J., Tajkhorshid, E., Fuller, G., Dunn, A. R., & Weis, W. I. (2019). Binding partner- and force-promoted changes in αE-catenin conformation probed by native cysteine labeling. *Scientific Reports*, *9*(1), 15375. https://doi.org/10.1038/s41598-019-51816-3

Thomas, W. A., Boscher, C., Chu, Y.-S., Cuvelier, D., Martinez-Rico, C., Seddiki, R., Heysch, J., Ladoux, B., Thiery, J. P., Mege, R.-M., & Dufour, S. (2013). α-Catenin and Vinculin Cooperate to Promote

High E-cadherin-based Adhesion Strength. *Journal of Biological Chemistry*, *288*(7), 4957–4969. https://doi.org/10.1074/jbc.M112.403774

Tuladhar, R., Yeu, Y., Tyler Piazza, J., Tan, Z., Rene Clemenceau, J., Wu, X., Barrett, Q., Herbert, J., Mathews, D. H., Kim, J., Hyun Hwang, T., & Lum, L. (2019). CRISPR-Cas9-based mutagenesis frequently provokes on-target mRNA misregulation. *Nature Communications*, *10*(1), 4056. https://doi.org/10.1038/s41467-019-12028-5

Twiss, F., le Duc, Q., van der Horst, S., Tabdili, H., van der Krogt, G., Wang, N., Rehmann, H., Huveneers, S., Leckband, D. E., & de Rooij, J. (2012). Vinculin-dependent Cadherin mechanosensing regulates efficient epithelial barrier formation. *Biology Open*, *1*(11), 1128–1140. https://doi.org/10.1242/bio.20122428

van den Goor, L., & Miller, A. L. (2022). Closing the gap: Tricellulin/α-catenin interaction maintains epithelial integrity at vertices. *Journal of Cell Biology*, *221*(4). https://doi.org/10.1083/jcb.202202009

Wang, A., Dunn, A. R., & Weis, W. I. (2022). Mechanism of the cadherin-catenin F-actin catch bond interaction. *ELife*, *11*. https://doi.org/10.7554/eLife.80130

Xu, X.-P., Pokutta, S., Torres, M., Swift, M. F., Hanein, D., Volkmann, N., & Weis, W. I. (2020). Structural basis of αE-catenin-F-actin catch bond behavior. *ELife*, *9*. https://doi.org/10.7554/eLife.60878

Yao, M., Qiu, W., Liu, R., Efremov, A. K., Cong, P., Seddiki, R., Payre, M., Lim, C. T., Ladoux, B., Mège, R.-M., & Yan, J. (2014). Force-dependent conformational switch of α-catenin controls vinculin binding. *Nature Communications*, *5*(1), 4525. https://doi.org/10.1038/ncomms5525

Yonemura, S., Wada, Y., Watanabe, T., Nagafuchi, A., & Shibata, M. (2010). α-Catenin as a tension transducer that induces adherens junction development. *Nature Cell Biology*, *12*(6), 533–542. https://doi.org/10.1038/ncb2055

Zacharias, D. A., Violin, J. D., Newton, A. C., & Tsien, R. Y. (2002). Partitioning of Lipid-Modified Monomeric GFPs into Membrane Microdomains of Live Cells. *Science*, *296*(5569), 913–916. https://doi.org/10.1126/science.1068539